

## Plumes: Response of time migration to lateral velocity variation

Dimitri Bevc\*, James L. Black<sup>‡</sup>, and Gopal Palacharla\*\*

### ABSTRACT

We analyze how time migration mispositions events in the presence of lateral velocity variation by examining the impulse response of depth modeling followed by time migration. By examining this impulse response, we lay the groundwork for the development of a remedial migration operator that links time and depth migration. A simple theory by Black and Brzostowski predicted that the response of zero-offset time migration to a point diffractor in a  $v(x, z)$  medium would be a distinctive, cusp-shaped curve called a plume. We have constructed these plumes by migrating synthetic data using several time-migration methods. We have also computed the shape of the plumes by two geometrical construction methods. These two geometrical methods compare well and explain the observed migration results.

The plume response is strongly influenced by migration velocity. We have studied this dependency by migrating synthetic data with different velocities. The observed velocity dependence is confirmed by geometrical construction. A simple first-order theory qualitatively explains the behavior of zero-offset time migration, but a more complete understanding of migration velocity dependence in a  $v(x, z)$  medium requires a higher order finite-offset theory.

### INTRODUCTION

Time migration algorithms do not yield the correct image when velocity varies laterally. The correct image is best obtained by prestack depth migration. By studying the errors in time migration, it may be possible to establish an algorithmic link between time migration and depth migration. This is desirable since time migration is widely used, robust, well-

understood, and much faster than depth migration. In this paper, we study a point diffractor to examine the impulse response of depth modeling followed by time migration in the presence of lateral velocity variation. One motivation is to help interpreters better identify situations in which depth migration is required. A more ambitious motivation is to lay the groundwork for the development of an algorithmic connection between time and depth migrations, which we call *remedial migration*. Just as residual migration (Rothman et al., 1985) aims to correct errors in the velocity model, remedial migration would correct for errors in the time migration method.

The image-ray method of converting time-migrated images to depth is not valid for steeply dipping events and large velocity gradients. Hubral (1977) argued that the image ray connects time migration with depth migration. He began his argument with the implicit assumption that time migration moves an event to the apex of the true-diffraction curve, the zero-offset response to a point diffractor. The apex of the true-diffraction curve is located at the end of the image ray, that is the ray that strikes the earth's surface at normal incidence. Since the image ray connects the top of the true-diffraction curve with the subsurface point, Hubral argued that the image ray is the connection between time and depth migration. A correction method based on this view of the image ray has been applied to time-migrated data (Larner et al., 1981; Hatton et al., 1981). This correction fails for steeply dipping events. This failure results because time migration moves an event to the apex of the *time-migration* curve, which is not the same as the true-diffraction curve for a medium with lateral velocity variation (Black and Brzostowski, 1994). The two curves agree closely only for a limited range of dips corresponding to the apex of the true-diffraction curve.

To study the effect of lateral velocity gradients on 2-D zero-offset time migration, we have used a simple dipping-layer earth model. Earlier efforts have quantified the effects of velocity gradients by developing a first-order theory in

Manuscript received by the Editor November 10, 1993; revised manuscript received August 19, 1994.

\*Stanford Exploration Project, Department of Geophysics, Stanford University, Stanford, CA 943052215.

‡International Business Machines Corp., 1505 LBJ Freeway, Dallas, TX 75234.

\*\*Stanford Exploration Project, Department of Geophysics, Stanford University, Stanford, CA 94305-2215.

© 1995 Society of Exploration Geophysicists. All rights reserved.

terms of the strength of the lateral velocity variation (Black and Brzostowski, 1994). According to that theory, the impulse response of depth modeling followed by time migration in the presence of lateral velocity variation is a distinctive cusp-like shape that we call a *plume*. To study the nature of the plume beyond the limitations of the first-order theory, we have made two geometrical constructions based on point diffractor ray-tracing: superposition of semicircles and summation along hyperbolas. The plume shapes derived by these two techniques are consistent with experimental results obtained by time migrating a synthetic point diffractor response. The shape and location of the plume is not as simple as predicted by Black and Brzostowski's first-order theory, but it can be explained using ray-tracing and geometrical constructions.

Because the choice of migration velocity is critical, it is interesting to study the effect of migration velocity on the plume response in a  $v(x, z)$  medium. In practice, it is usually difficult to devise an accurate velocity for migration. For depth migration, it is generally accepted that the best available choice is a velocity that optimally focuses the image. But what happens when we use time migration to focus the image? We often employ time migration to image events when lateral velocity variations are present. In these situations, it is generally impossible to focus the image completely even when the correct velocity is used. We use both a geometrical construction and actual migrations of synthetic data to demonstrate the response of time migration in such a medium. In each case, the plume response rotates and changes shape with changing migration velocity. To gain some insight into this behavior, we have developed a simple first-order theory of plume rotation analogous to Black and Brzostowski (1994).

### GEOMETRICAL CONSTRUCTION OF PLUMES

To determine the shape of the plume, we first present two geometrical constructions based on semicircle superposition and hyperbola summation.

#### Dipping-layer model

The model used in this paper is displayed in Figure 1. An implicit velocity gradient is caused by the dipping layer since the velocity changes across it. We begin our study by analyzing the response of a point diffractor positioned below the layer. The parameters of the model were chosen to match the synthetic data example given by Black and Brzostowski (1994). The point diffractor is positioned at a depth of 1.22 km and a horizontal position of 2.44 km. Black and Brzostowski quantified time-migration errors for this model and for an earth model with a linear velocity gradient in the  $x$ -direction.

The true-diffraction curve for this model is the zero-offset response to a point diffractor. Exact ray-tracing with equations (A-4) and (A-5) of Appendix A shows that this curve is asymmetric (Figure 2). The arrival times are later where the low velocity wedge is thicker and earlier where the wedge is thinner. The apex of the curve is offset to the right of the diffractor position. This is shown more clearly in a closeup (Figure 3).

#### Semicircle superposition

Time migration may be thought of as hyperbola summation or semicircle superposition (Schneider, 1978). To illustrate the kinematics of time migration when there are lateral velocity variations, we first superimpose time-migration semicircles along the diffraction curve. This geometrical construction is shown in Figure 2, where the radius of each circle is determined by the rms velocity that would be derived from a well drilled straight down to the diffractor from the surface. This value is 2.7 km/s and is what we call the rms well velocity. This is the migration velocity used

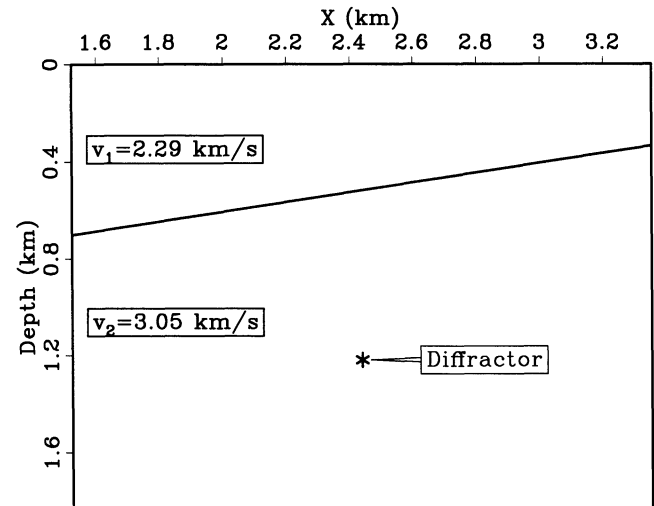


FIG. 1. Dinning-layer model. The change in velocity across the dipping layer causes an implicit velocity gradient that depends on the dip of the layer. For our examples we use a dip of  $11^\circ$ .

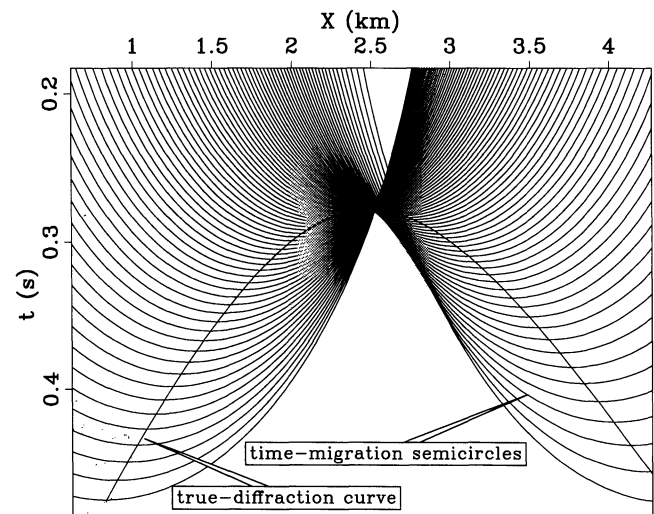


FIG. 2. The true-diffraction curve for the dipping-layer model is an asymmetric curve. Arrival times are later on the left than on the right because the low velocity wedge is thicker on the left. Time-migration semicircles are superimposed on the true-diffraction curve for the dipping-layer model. The points where the semicircles add constructively form the migrated image.

throughout this paper. The points at which the semicircles add constructively, form the time-migrated image of the point diffractor. Figure 3 is an enlarged view showing the semicircle superposition near the apex of the true-diffraction curve. The envelope of semicircles is displaced to the right of the true diffractor position at 2.44 km and forms a distinctive cusp shape that opens to the right. This shape is what we call the plume. The plume shows that the various dip components of a point diffractor end up at different positions on the time-migrated image. Thus the plume shows clearly that misfocusing occurs when time migration is applied to a medium with lateral velocity variations.

The plume shape can be qualitatively explained by examining the kinematics of time migration. For the left side of the true-diffraction curve, the migration velocity is too fast, so that the limb of the curve is over-migrated. For the right side of the true-diffraction curve, the migration velocity is too slow, so that the limb of the curve is undermigrated.

**Hyperbola summation**

The semicircle superposition method allows us to visualize how the plume is built up from constructive interference. It does not, however, offer a convenient way to compute the actual shape of the plume numerically. A more effective way to compute the time-migration response to a point diffractor is by summing along hyperbolas (Schneider, 1978). The analytical technique for summing along hyperbolas is called the common-tangent construction. It relies on the fact that the main contribution to the sum comes from the place where a time-migration hyperbola is tangent to the true-diffraction curve of Figure 2. The event at the tangency point is positioned by time migration to the apex of the time-migration hyperbola.

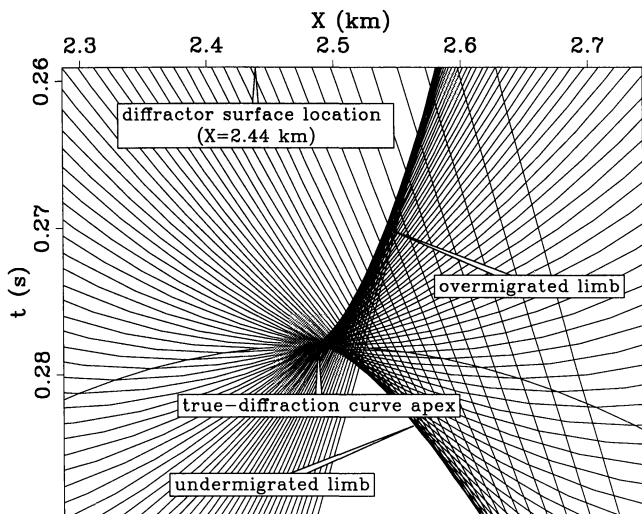


FIG. 3. Enlargement of the time-migration semicircles superimposed along the true-diffraction curve. The apex of the true-diffraction curve is offset to the right of the diffractor surface location. The envelope of semicircles forms a plume with overmigrated and undermigrated limbs.

The time-migration hyperbola is given by:

$$t_0^2 = t_k^2 + 4 \left[ \frac{x_0 - x_k}{V(x_m, t_m)} \right]^2, \tag{1}$$

where  $V(x_m, t_m)$  is the rms well velocity at the diffractor location. Matching the slope of the hyperbola given by equation (1) with the time dip  $D$  of the event leads to the following formulas for the position of the time-migrated point  $(x_k, t_k)$ :

$$x_k = x_0 - \left[ \frac{V(x_m, t_m)D}{2} \right] \left[ \frac{V(x_m, t_m)t_0}{2} \right], \tag{2}$$

$$t_k = t_0 \sqrt{1 - \left[ \frac{V(x_m, t_m)D}{2} \right]^2}, \tag{3}$$

where

$$D = \frac{\partial t_0}{\partial x_0}$$

is the apparent time dip of the event to be migrated.

This procedure is carried out for each point along the true-diffraction curve to yield the complete response of time migration to a point diffractor. Details regarding the algebra of this computation are given in Appendix A, and the results are shown in Figure 4. In generating this figure we again have used the vertical rms well velocity that was used in Figure 2. Note that the plume envelope in Figure 3 matches the curve in Figure 4 exactly. Thus the two ways of geometrically constructing the time-migration response to lateral velocity variation are consistent.

**SYNTHETIC MODELING AND MIGRATION**

To confirm the geometric construction of plumes, we now turn to wave-equation synthetic experiments on a point diffractor beneath the lateral velocity variation shown in Figure 1. A Kirchhoff modeling program was used to gener-

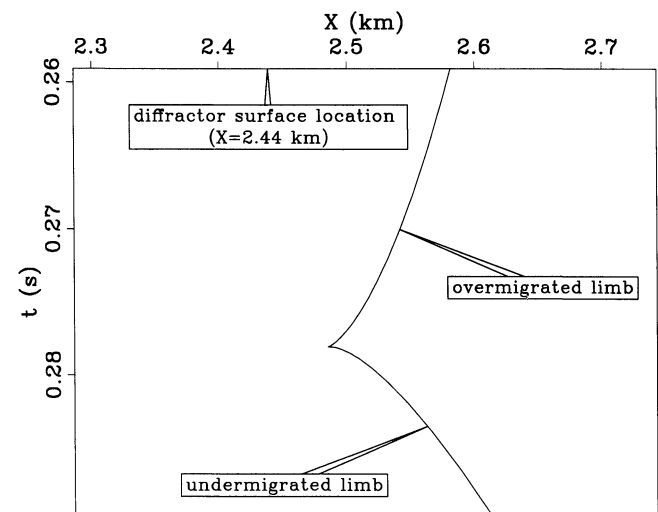


FIG. 4. Plume derived by hyperbola summation with the common-tangent construction. This curve corresponds to the envelope of semicircles in Figure 3 exactly.

ate synthetic data for time migration. The resulting asymmetric diffraction curve is displayed in Figure 5a. The Kirchhoff migrated image in Figure 5b was generated from this diffraction curve using the rms well velocity that would be derived from a vertical well over the diffractor, as before. Note the distinctive plume response evident in this figure. The common-tangent result is superimposed on the migrated image, showing that the agreement between wave-equation results and geometrical predictions is excellent.

The above wave-equation evidence for plumes relies upon the Kirchhoff migration technique, which is closely related to our geometrical constructions. It is of interest to see whether the plume shape appears when other types of time migration are used. Thus we present Stolt (1978) and Gazdag (1978) phase-shift migration images of the point diffractor in Figure 5c and Figure 5d, respectively. Both the Stolt and Gazdag results were obtained using a constant rms well velocity having the same value as shown in Figure 5b. Notice that in both cases we obtain plume shapes that are in good agreement with our geometrical constructions and with the Kirchhoff result of Figure 5b.

### PLUME VARIATION WITH MIGRATION VELOCITY

In practice, it is difficult to choose the correct velocity for migration. It is therefore instructive to see what effect the variation of migration velocity has on plumes in a  $v(x, z)$  medium. In this section, we demonstrate the effects of migration velocity on plume shape and formation by migrating synthetic data and by geometrical construction.

### Observed effect of migration velocity changes

The synthetic data from Figure 5a are migrated with a Kirchhoff algorithm using various migration velocities and are displayed in Figure 6. Each frame is migrated using a different constant velocity. The velocities used are 2.3 km/s to 3.5 km/s in increments of 0.15 km/s. The image changes from undermigrated in the upper left corner to overmigrated in the lower right corner. The fourth frame ( $V_{mig} = 2.75$ ) is migrated with a velocity close to the rms well velocity (2.7 km/s) used in Figure 5b.

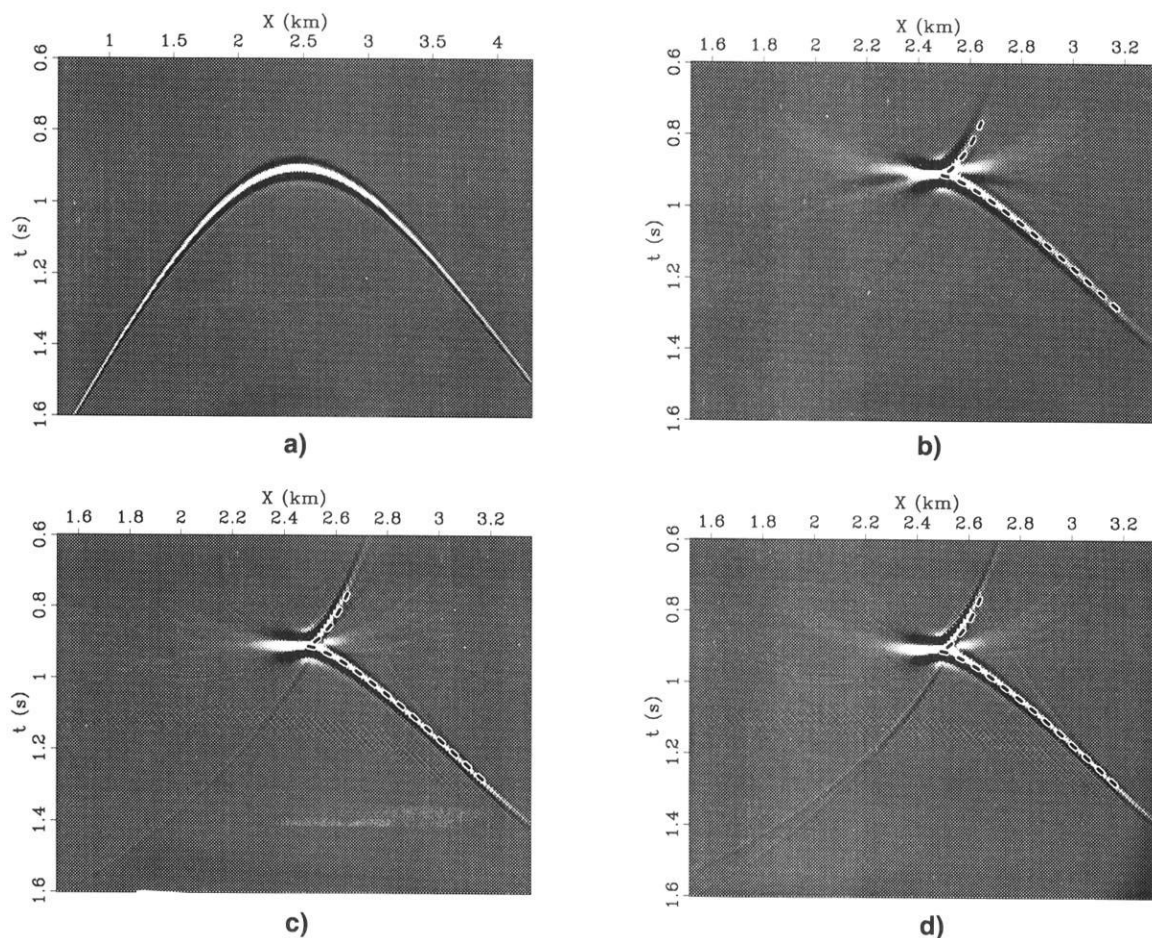


FIG. 5. Synthetic modeling and migration: (a) Kirchhoff modeling result for the point diffractor model. The kinematics correspond to the ray-tracing result shown in Figure 2. This synthetic data is the input to the following three migration results. (b) Comparison of the Kirchhoff migration result and the tangent construction. (c) Comparison of the Stolt migration result and the tangent construction. (d) Comparison of the Gazdag phase-shift migration result and the tangent construction.

As migration velocity is increased, the image begins to develop an upper limb. This upper limb becomes evident in the third frame ( $V_{mig} = 2.6$ ) of Figure 6. The plume is well formed in the fourth frame ( $V_{mig} = 2.75$ ) and then appears to rotate clockwise as migration velocity is increased. In the last frame, the lower limb of the plume is very faint and the image looks overmigrated.

By scrutinizing the frames of the movie in Figure 6, we can see how the plume is formed. The left limb of the undermigrated image in frame 1 ( $V_{mig} = 2.3$ ) gets swept upward and becomes the upper limb of the plume in frame 4 ( $V_{mig} = 2.75$ ). Recall that the low velocity wedge (Figure 1) has the effect of making the left side of the true-diffraction curve overmigrated when the rms well velocity is used. This overmigration sweeps the limb upward. The right limb of the undermigrated image in frame 1 ( $V_{mig} = 2.3$ ) remains undermigrated as velocity increases until the last few frames where the typical overmigration smile begins to form.

### Agreement with geometrical construction

To gain some intuition into the formation of the plume as a function of migration velocity, the tangent construction method can be compared to the result of migrating the synthetic data. In Figure 7 the plume variation with migration velocity is examined for a smaller range of migration velocity than in Figure 6. The center frame ( $\Delta V_{mig} = 0.0$ ) is migrated with the rms well velocity of 2.7 km/s. The image in the first two frames is a characteristic undermigration frown, and the image in the last frame is a characteristic overmigration smile. As in Figure 6, we can see the left side of the diffraction curve being swept up to form the upper limb of the plume while the right side of the diffraction curve eventually forms the left side of the smile. Migration velocities close to the rms well velocity, frames 3 ( $\Delta V_{mig} = -0.06$ ) through 7 ( $\Delta V_{mig} = 0.06$ ), show the plume rotating

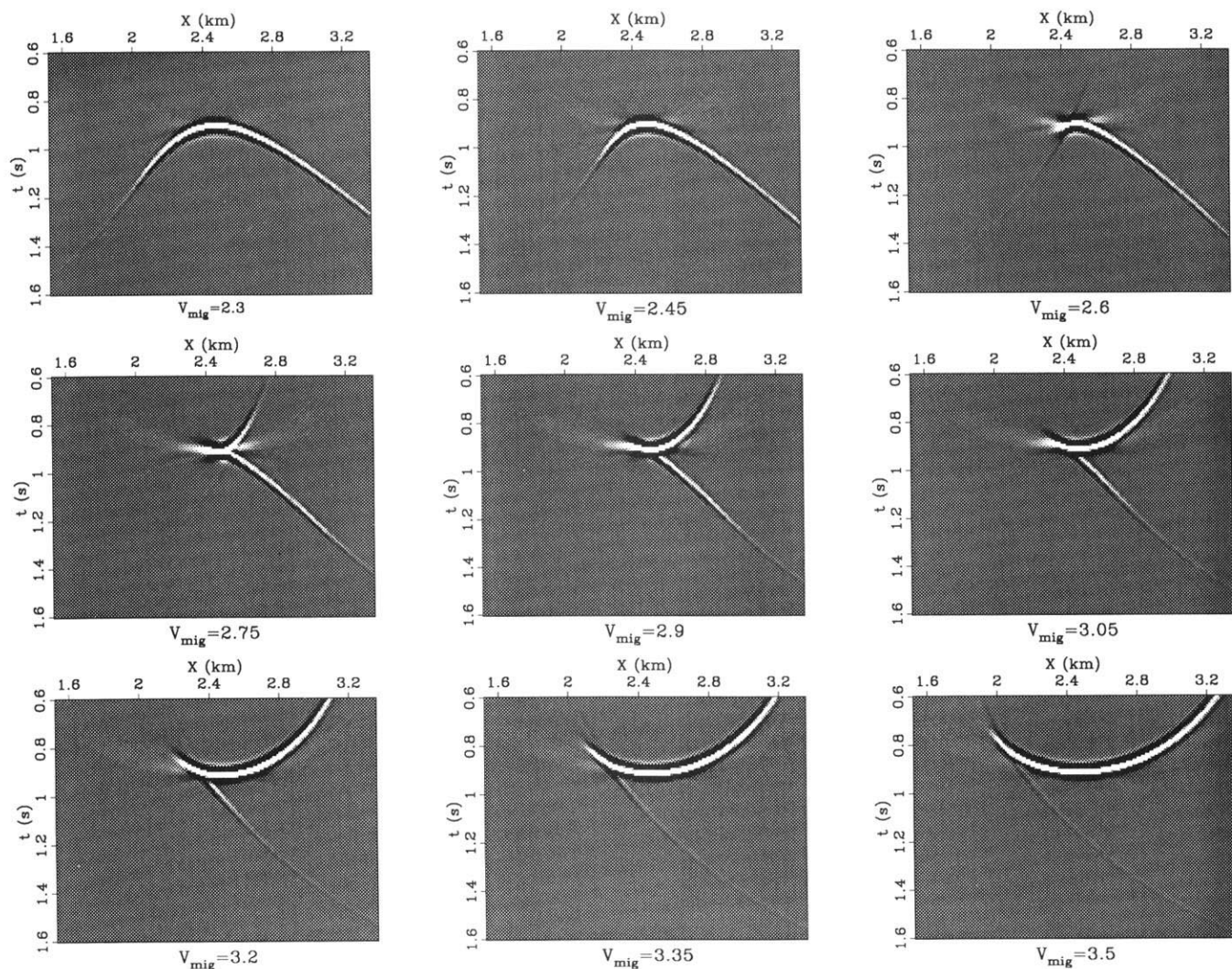


FIG. 6. Kirchhoff migration with a range of velocities. The constant migration velocity ranges from 2.3 km/s to 3.5 km/s. The rms well velocity at the diffractor position is 2.7 km/s.

slightly clockwise, although the overall rotation trend evident in frames 2 through 8 is somewhat counterclockwise.

As is evident from the overlays of Figure 7, the tangent construction method is in good agreement with the synthetic result.

**FIRST-ORDER KINEMATICS OF PLUMES**

In this section, we review Black and Brzostowski's (1994) first-order theory of plumes, and we present a first-order theory of plume velocity dependence. We compare both these theoretical results to the modeling results of previous sections.

**First-order theory of plumes**

The geometry used for the derivation of the theoretical result is illustrated in Figure 8. Starting at the point diffractor location  $(x_m, z_m)$ , a normal ray is traced to the surface where it emerges at  $x_0$ . Time migration then translates us to

the point  $x_k$ . Black and Brzostowski go on from  $x_k$  along the image ray to the point  $Q$ . The difference between  $Q$  and  $(x, z_m)$  is the error after the image ray correction. Since we are concerned with the response of time migration to lateral velocity variation, we are interested in the time-migrated position  $(x_k, t_k)$ .

The velocity gradient that gives rise to the plumes is caused by the velocity contrast across the dipping layer and the dip angle  $\theta_1$ . To simplify the analysis, velocity contrast is defined as

$$\gamma = \frac{v_2 - v_1}{v_2}$$

Black and Brzostowski (1994) express the true-diffraction curve to first order in  $\gamma$  and  $\sin \theta_1$  and then perform time migration by common-tangent construction. By matching the slope of the time-migration hyperbola to the time dip  $D$  of the true-diffraction curve and expanding to first order in  $\gamma$

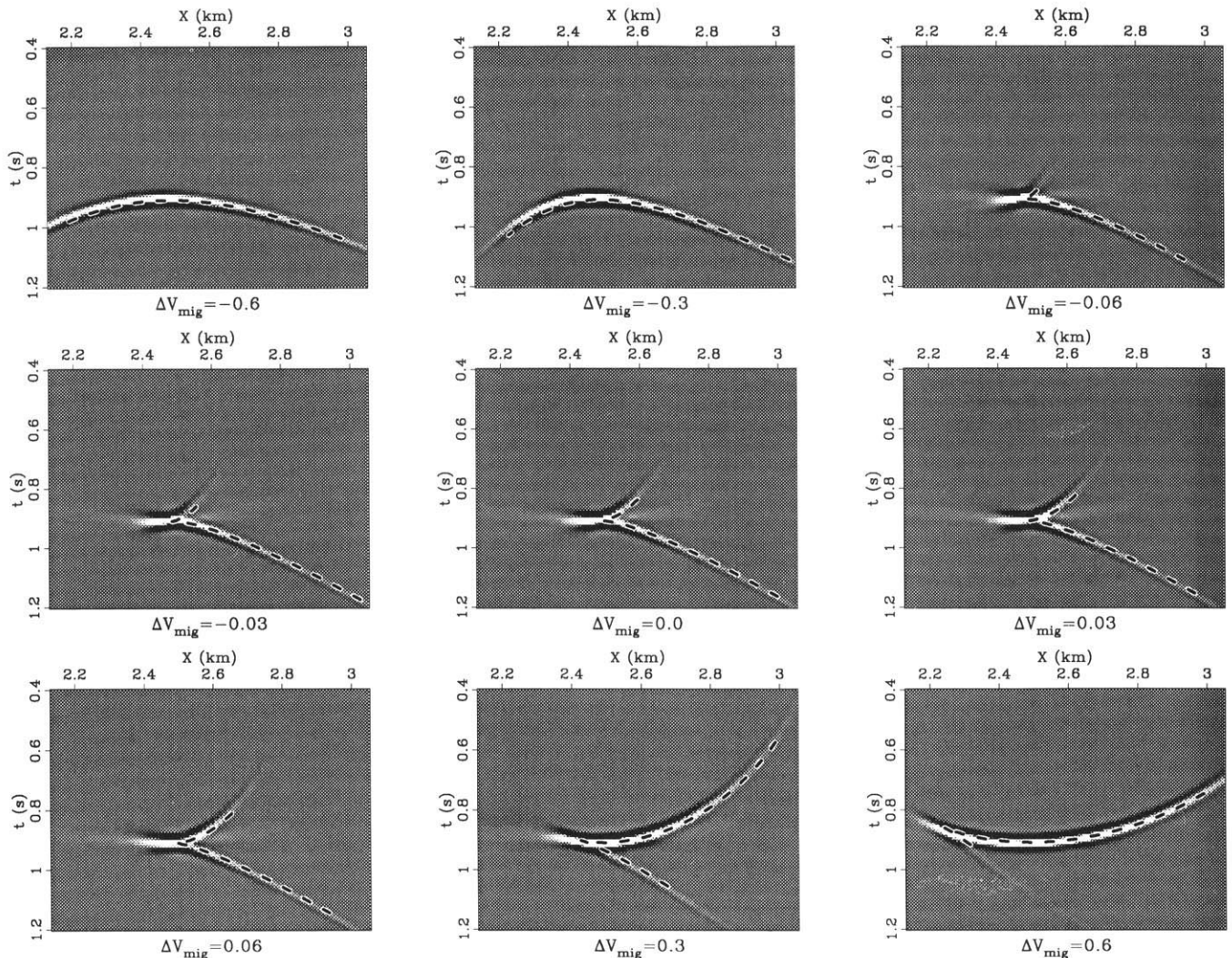


FIG. 7. Kirchhoff migration with various migration velocities overlain by the results of the tangent construction method. The center frame is migrated with the rms well velocity of 2.7 km/s. The other frames are migrated with velocities of  $V_{mig} = V_{rms} + \Delta V_{mia}$ . The  $\Delta V_{mia}$  values are given at the bottom of each frame in units of km/s.

and  $\sin \theta_1$  they obtain the spatial and temporal position of the event after time migration:

$$x_k \approx x_m + A(x_m, z_m)(1 + 3 \tan^2 \theta), \quad (4)$$

$$\frac{v_2 t_k}{2} \approx \frac{v_2 t_m}{2} - 2A(x_m, z_m) \tan' \theta. \quad (5)$$

The quantity  $A$  embodies the parameters that contribute to the effective velocity gradient and is defined as:

$$A(x_m, z_m) = d_2 \gamma \sin \theta_1.$$

We can vary  $\theta$  in equations (4) and (5) to get a first-order analytic representation for the plume. This is done for propagation angles of  $\pm 60^\circ$  in Figure 9. This theoretical result is well positioned relative to the synthetic result. The synthetic plume is skewed upwards whereas the theoretical plume is symmetric about a horizontal axis drawn through its apex. The theoretical plume does not overlie the synthetic result exactly. However, both the theoretical and synthetic plume open in the same direction and display the same type of limb curvature: convex upward on the upper limb and convex downward on the lower limb.

Although the first-order theory contains some of the features of the plume, it is incomplete. It is clear that a higher-order theory is needed to explain all the features of time-migration plumes.

**First-order theory of plume velocity dependence**

We now present a first-order theory for plume velocity dependence. As before, we use the geometry of Figure 8 as the basis of our derivation and we retain only terms to first

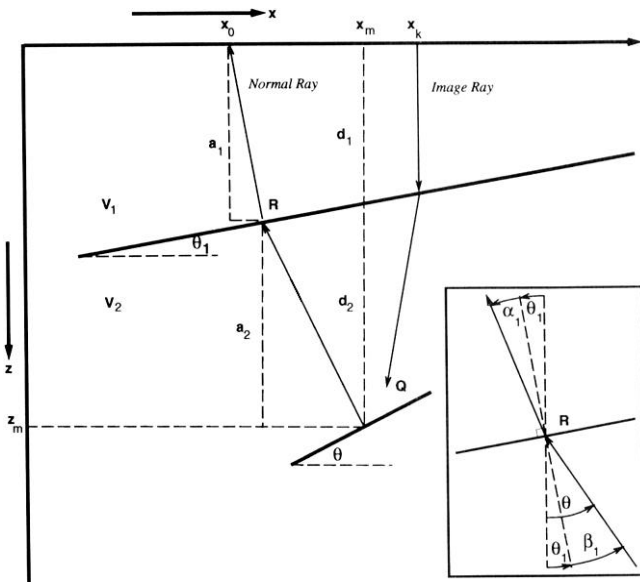


FIG. 8. Geometry and raypaths for the dipping layer model. The diffractor is positioned at  $(x_m, z_m)$ . The spatial and temporal coordinates of the diffraction curve and time-migrated image are given by  $(x_0, z_0)$  and  $(x_k, z_k)$ , respectively.

order in  $\gamma$  and  $\sin \theta_1$ . The details of the derivation are presented in Appendix B.

We define a migration velocity  $V_{mig}$  that differs from the rms well velocity  $V(x_m, t_m)$  by

$$\Delta V_{mig} = V_{mig} - V(x_m, t_m).$$

For small values of  $\Delta V_{mig}$ , such that

$$\frac{\Delta V_{mig}}{V(x_m, t_m)} \leq \gamma,$$

we can express the first-order theory for a perturbation in migration velocity by the following equations:

$$x_k = x_m + A(1 + 3 \tan^2 \theta) + \frac{2\Delta V_{mig}}{V_{mig}} z_m \tan \theta, \quad (6)$$

$$\frac{v_2 t_k}{2} = \frac{v_2 t_m}{2} - 2A \tan^3 \theta - \frac{\Delta V_{mig}}{V_{mig}} z_m \tan^2 \theta. \quad (7)$$

The theoretical curves given by equations (6) and (7) are plotted in Figure 10 for the same values of migration velocity that are used in Figure 7. Notice that if  $\Delta V_{mig} = 0$  equations (6) and (7) reduce to equations (4) and (5). The center frame of Figure 10 ( $\Delta V_{mig} = 0$ ) is generated using the rms well velocity. It is the same as the first-order curve overlaid on the migration result in Figure 9.

The first-order theory does not match the tangent construction and Kirchhoff migration (Figure 7) results exactly; however, we can qualitatively follow the plume formation in Figure 10 just as we did in the other two cases. The curve progresses from an undermigrated frown to an overmigrated smile as the migration velocity increases. It is evident how the left limb of the frown curls around to form the upper limb of the plume ( $\Delta V_{mig} = -0.06$ ) and later, as velocity increases even more, into the right side of the smile ( $\Delta V_{mig} = 0.3$ ). Similarly, the right limb of the frown

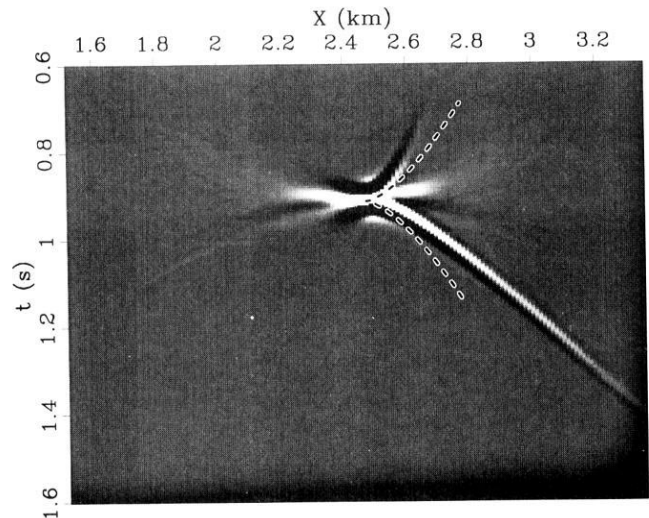


FIG. 9. Comparison of the analytic expression for the plume to the Kirchhoff migration result. The migration result is identical to Figure 5b, but here we overlay the theoretical result derived by Black and Brzostowski (1994).

becomes the lower limb of the plume, and as velocity increases, it becomes the left side of the smile. We do not observe the slight clockwise rotation in the three middle frames with this simple first-order theory. To more fully understand the velocity dependence of plumes in  $v(x, z)$  media, a higher order finite-offset theory is needed.

### CONCLUSIONS

The results of the geometrical construction methods confirm the existence of plumes and give insight into how and why they form. These results match the three synthetic time migration results very well. We have demonstrated that the first-order theory developed by Black and Brzostowski (1994) and the first-order theory of velocity dependence qualitatively describe the plume response. However, a higher order theory is needed to explain the kinematics more exactly.

By examining the impulse response of depth modeling followed by time migration, we have laid the groundwork for the development of a remedial migration operator that links time and depth migration. The next step in this study will be to use an operator based on the plume response to turn a time-migrated output into a depth-migrated output. This is desirable since time migration is much faster and more robust than depth migration. Although the combination of time migration and remedial migration may not replace depth migration entirely, it could serve as a tool for migration velocity estimation.

By being aware of the mispositioning error that occurs with time migration in laterally variable media, interpreters can better judge when depth migration is needed. Using equations (4) and (5) it is possible to make back-of-the-envelope calculations to estimate how severe the mispositioning caused by migration may be for a given velocity structure.

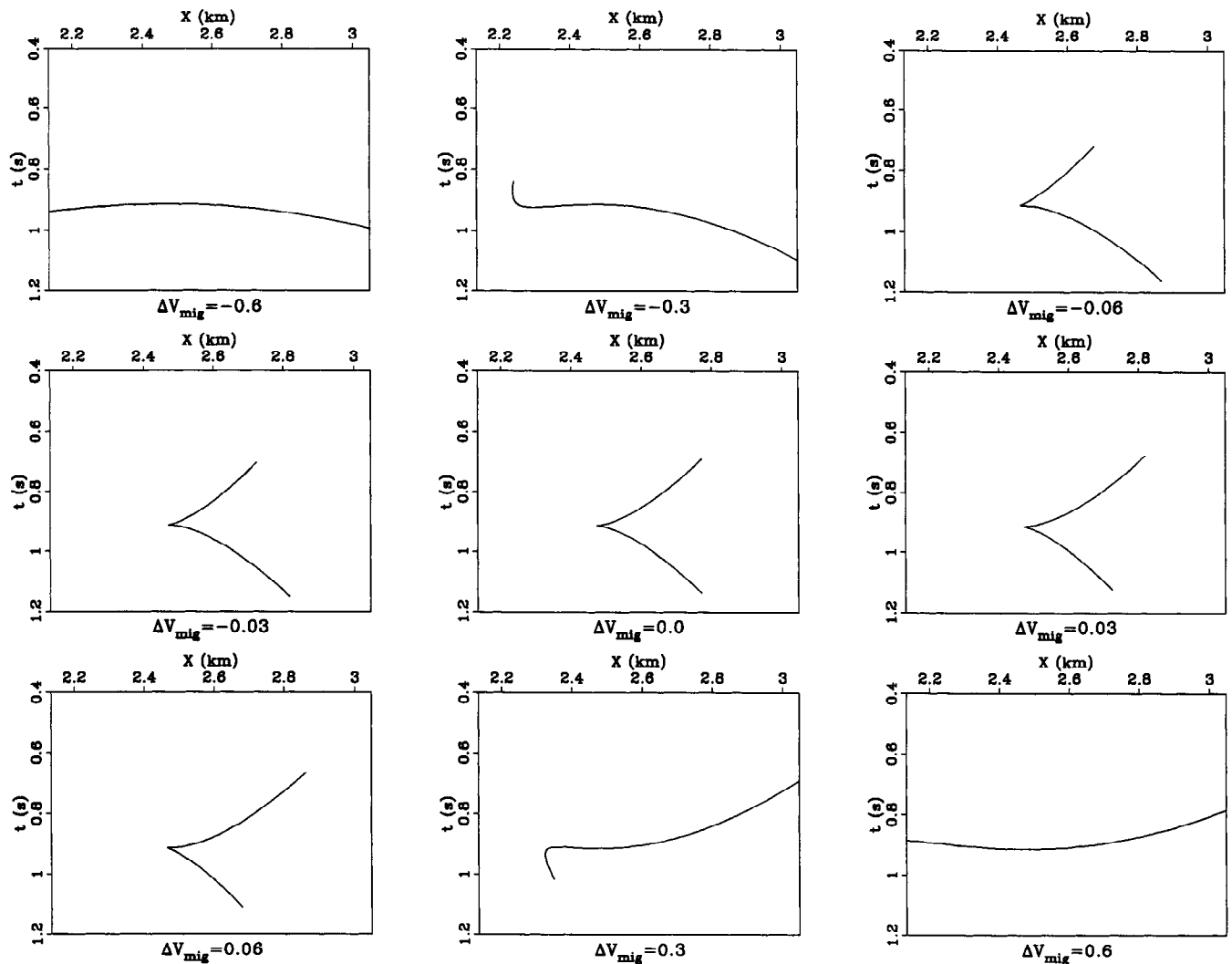


FIG. 10. First-order theory of plume velocity dependence. The same migration velocities used in Figure 7 are used here. The center frame  $\Delta V_{\text{mig}} = 0.0$  is generated using the rms well velocity of 2.7 km/s. It is the same curve that is overlain on Figures 9.

## ACKNOWLEDGMENTS

We would like to thank Lin Zhang, Jon Claerbout, Lewei MO, and Matt Brzostowski for their suggestions and discussions. Jim Black wishes to express his gratitude to IBM for allowing him to spend time at Stanford where most of this work was done. The quality of the paper was improved during the review process by comments from Stew Levin, Keh Pann, and Andreas Ehinger.

## REFERENCES

Black, J. L., and Brzostowski, M. A., 1994, Systematics of time-migration errors: *Geophysics*, 59, 1419-1434.

Gazdag, J., 1978, Wave equation migration with the phase shift method: *Geophysics*, 43, 1342-1351.  
 Hatton, L., Larner, K. L., and Gibson, B. S., 1981, Migration of seismic data from inhomogeneous media: *Geophysics*, 46, 751-767.  
 Hubral, P., 1977, Time migration-some ray theoretical aspects: *Geophys. Prosp.*, 25, 738-745.  
 Larner, K. L., Hatton, L., and Gibson, B. S., 1981, Depth migration of imaged time sections: *Geophysics*, 46, 734-750.  
 Rothman, D. H., Levin, S. A., and Rocca, F., 1985, Residual migration-applications and limitations: *Geophysics*, 50, 110-126.  
 Schneider, W. A., 1978, Integral formulation for migration in two-dimensions and three-dimensions: *Geophysics*, 43, 49-76.  
 Stolt, R. H., 1978, Migration by Fourier transform: *Geophysics*, 43, 23-48.

## APPENDIX A

## TANGENT CONSTRUCTION

In this Appendix, we derive the formulas used to obtain the ray-tracing results for the dipping layer model and the tangent construction migration.

The first step is to model the asymmetric true-diffraction curve. This is done by applying Snell's law at the point  $R$  where the normal ray crosses the interface in Figure 8. Snell's law at  $R$  is given by

$$\frac{\sin \alpha_1}{v_1} = \frac{\sin \beta_1}{v_2}, \quad (\text{A-1})$$

where  $\alpha_1$  and  $\beta_1 = \theta - \theta_1$  are the angles of incidence above and below the interface. The vertical distances ( $a_1, a_2$ ) are expressed in terms of the vertical distances ( $d_1, d_2$ ) at the migrated position. From the geometry of Figure 8 we get

$$d_1 = a_1 - a_2 \tan \theta \tan \theta_1 \quad (\text{A-2})$$

and

$$d_2 = a_2 + a_2 \tan \theta \tan \theta_1. \quad (\text{A-3})$$

We now wish to derive the horizontal deviation of the normal ray. From Figure 8, we see that this is the sum of two terms:

$$x_0 - x_m = -a_1 \tan(\theta_1 + \alpha_1) - a_2 \tan \theta. \quad (\text{A-4})$$

The traveltimes along the normal ray is given by

$$t_0 = \frac{2a_1}{v_1 \cos(\theta_1 + \alpha_1)} + \frac{2a_2}{v_2 \cos \theta}. \quad (\text{A-5})$$

The apparent time dip  $D$  at the earth's surface is given by

$$D = -\frac{2 \sin(\theta_1 + \alpha_1)}{v_1}. \quad (\text{A-6})$$

Equations (A-4) and (A-5) define the true-diffraction curve (Figure 2).

Common-tangent migration is performed by matching the time dip  $D$  of equation (A-6) with the dip of the time-migration curve and moving the point to the apex of the time-migration curve. Carrying out this procedure as discussed in the main text results in Figure 4.

## APPENDIX B

## FIRST-ORDER THEORY OF PLUME VELOCITY DEPENDENCE

The first-order theory of plume velocity dependence is developed here using similar reasoning to Black and Brzostowski's (1994) first-order theory.

We begin with the zero-offset time-migration curve:

$$t_0^2 = t_k^2 + 4 \left[ \frac{x_0 - x_k}{V_{mig}} \right]^2, \quad (\text{B-1})$$

where  $(x_k, t_k)$  are the coordinates of the time-migrated point and  $V_{mig}$  is the migration velocity. Defining the velocity contrast across the dipping reflector as

$$\gamma = \frac{v_2 - v_1}{v_2},$$

and the dip angle as  $\theta_1$ , Black and Brzostowski (1994) use the geometry of Figure 8 to express the true-diffraction curve to first order in  $\gamma$  and  $\sin \theta_1$  as:

$$x_0 - x_m \approx -z_m \tan \theta + \gamma d_1 \frac{\sin \theta}{\cos^3 \theta} - \gamma \sin \theta_1 z_m \frac{1}{\cos^4 \theta} + A \frac{1 + \sin^2 \theta}{\cos^4 \theta}, \quad (\text{B-2})$$

$$\frac{v_2 t_0}{2} \approx \frac{z_m}{\cos \theta} + \gamma d_1 \frac{1 - 2 \sin^2 \theta}{\cos^3 \theta} + \gamma \sin \theta_1 z_m \frac{\sin \theta}{\cos^4 \theta} - 2A \frac{\sin^3 \theta}{\cos^4 \theta}, \quad (\text{B-3})$$

where the quantity  $A$  is defined as

$$A(x_m, z_m) = d_2 \gamma \sin \theta_1.$$

By varying  $\theta$ , equations (B-2) and (B-3) define a diffraction curve like that given in Figure 2. The first term of the equations yields the constant velocity hyperbola, the second term contains the effects of vertical velocity gradients, the third and fourth terms contain the effects of lateral velocity changes.

Matching the slope of the time-migration curve, equation (B-1), with the time dip  $D$  of the true-diffraction curve leads to the following formulas for the position of the time-migrated point  $(x_k, t_k)$ :

$$x_k = x_0 - \left[ \frac{V_{mig} D}{2} \right] \left[ \frac{V_{mig} t_0}{2} \right], \quad (B-4)$$

$$t_k = t_0 \sqrt{1 - \left[ \frac{V_{mig} D}{2} \right]^2}, \quad (B-5)$$

where the time dip  $D$  can be expressed to first order in  $\gamma$  and  $\sin \theta_1$  as

$$\frac{v_2 D}{2} \approx -\sin \theta - \gamma \frac{\sin \theta_1}{\cos \theta}. \quad (B-6)$$

Black and Brzostowski (1994) define the rms velocity  $V(x_m, t_m)$  at the correct migrated position  $(x_m, t_m)$  to first-order in  $\gamma$  and  $\sin \theta_1$  as

$$\left[ \frac{V(x_m, t_m)}{v_2} \right]^2 \approx 1 - 2\gamma \frac{d_1}{z_m}. \quad (B-7)$$

This corresponds to the rms well velocity that we use throughout this paper.

Since we are interested in the variation of the plume operator with migration velocity, we define the perturbed migration velocity as

$$\begin{aligned} V_{mig} &= V(x_m, t_m) + \Delta V_{mig} \\ &= V(x_m, t_m) \left( 1 + \frac{\Delta V_{mig}}{V(x_m, t_m)} \right) \end{aligned} \quad (B-8)$$

Considering small values of  $\Delta V_{mig}$  so that

$$\frac{\Delta V_{mig}}{V(x_m, t_m)} \leq \gamma,$$

we can expand  $V_{mig}^2$  retaining only first-order terms as

$$V_{mig}^2 \approx V(x_m, t_m)^2 \left( 1 + 2 \frac{\Delta V_{mig}}{V(x_m, t_m)} \right). \quad (B-9)$$

Time migration is carried out by inserting equations (B-2), (B-3), (B-7), and (B-9) into equations (B-4) and (B-5). Retaining only the terms that are first order in  $\gamma$  and  $\sin \theta_1$  allows us to express the first-order theory for a perturbation in migration velocity by equations (6) and (7) of the main text.